Optimisation of a high speed rotating composite drive shaft using a genetic algorithm – Hybrid high modulus-high resistance carbon solutions

O. Montagnier[a,*], Ch. Hochard[b]

[a] *Écoles d'Officiers de l'Armée de l'air (EOAA), Centre de Recherche de l'Armée de l'air (CReA), BA 701, 13361 Salon Air, France*
[b] *Laboratoire de Mécanique et d'Acoustique (LMA), 31 chemin Joseph Aiguier, 13402 Marseille Cedex 20, France*

Abstract

This study deals with the optimisation of subcritical and supercritical laminated composite drive shafts, based on a genetic algorithm. The first part focuses on the modelling of a composite drive shaft. Flexural vibrations in a simply supported composite drive shaft mounted on viscoelastic supports, including shear effects are studied. In particular, an analytic stability criterion is developed to ensure the integrity of the system. The torsional strength is then computed with the maximum stress criterion, assuming the coupling effects to be null. Torsional buckling of thin walled composite tubes is modelled using a combination between laminate theory and Flügge theory. In the second part, the genetic algorithm is developed. The last part presents a comparative study between various composite materials solutions on a helicopter tail rotor driveline. In particular, hybrid tubes consisting of high modulus and high resistance carbon/epoxy plies are studied. These solutions make it possible to replace the conventional driveline consisting of five aluminium tubes by either three subcritical composite shafts or one supercritical composite shaft. The saving weight is equal to 42% and 72%, respectively. This study yielded some general rules for designing an optimum composite shaft which can be used without any optimisation algorithms.

Keywords:
drive shaft, hybrid composite laminate, rotordynamic, torsional buckling, optimisation, genetic algorithm

1. Introduction

Since the 1970s, composite materials have been regarded as potential candidates for manufacturing drive shafts of many kinds because of their high specific stiffness and strength [1]. Previous studies on this topic have dealt mainly with composite shaft design in the subcritical case, that is when the first critical speed is never exceeded. However, when a long driveline is required (in the case of helicopters, tiltrotors, tailless aircrafts with twin turboprops etc.), an additional means of increasing drive shaft length consists in to operating above this first critical speed, in the so-called supercritical regime. The main advantage of long shafts is that they reduce the number of bearing supports, and thus greatly decrease the maintenance costs and the driveline weight. The design process is more complex because the shaft has to go through a critical speed and dynamic instability due to rotating damping can occur in this regime. The aeronautic applications are suitable for operating in the supercritical regime because the driveline always rotates at a nominal speed during flight. Acceleration and deceleration operations are carried out on the ground. The aim of this paper is to optimise a supercritical drive shaft in this practical case.

Many different numerical optimisation methods have been used for designing composite drive shafts in order to reduce the weight, for example. Traditional methods based on the gradients of continuous functions have been used by several authors [2, 3, 4, 5]. These methods are unsuitable in the case of composite laminates, because many of the variables which have to be optimised are discrete variables (such as the number of plies) or discontinuous (such as the ply angle in classical manufacture process). It is therefore necessary to assume these variables to be continuous to be able to compute gradients. The optimisation techniques for solving problems involving discrete variables are known as metaheuristic methods. For example, Gubran and Gupta [6] have used simulated annealing techniques based on a neighbourhood approach. A review of the literature shows that genetic algorithms (GA) [7] are well adapted to designing laminate structures. GA were used for the first time to optimising a composite laminate in [8] and recently in the optimisation of a flexible matrix composite drive shaft in [9]. Here, it is proposed to use a GA with penalisation methods to account for the constraint functions. Additionally, in order to reduce CPU time, all design aspects are handled without the use of finite element methods.

In drive shaft applications, the choice of composite material is of great importance. Several authors have recommended the use of hybrid composites in the production of drive shafts. Brown and Rezin [10] and Xu et al. [11] studied the advantages of a mixture of glass fibres and carbon fibres in a modified epoxy matrix. Lee et al. [12] and Gubran [13] studied the design and manufacture of hybrid metallic/composite drive shafts. Here it is proposed to study a mixture of high modulus (HM) and high resistance (HR) carbon fibre plies. The aim is to benefit from the main advantages of

*Corresponding author. Tel. : (+33)04.90.17.80.93 ; fax : (+33)04.90.17.81.89.
Email address: olivier.montagnier@inet.air.defense.gouv.fr (O. Montagnier)

Nomenclature

A, A_{ij}	in-plane stiffness matrix of the laminate and elements of the matrix ($i, j = 1,2,6$)
a, a_{ij}	in-plane compliance matrix of the laminate and elements of the matrix
B, B_{ij}	coupling stiffness matrix of the laminate and elements of the matrix
bit	discrete quantity of bits
c	viscous damping
D, D_{ij}	flexural stiffness matrix of the laminate and elements of the matrix
e	thickness
E	longitudinal Young's modulus of the shaft
E_{11}, E_{22}, E_{12}, E_{44}, E_{55}, E_{66}	longitudinal and transverse Young's modulus, Poisson's ratio, out-of-plane (transverse / normal, longitudinal / normal) and in-plane shear modulus of the ply
f	fitness function
G	transverse shear modulus of the shaft
g	constraint function
I_x	polar area moment of inertia of the shaft
I_y, I_z	transverse area moments of inertia of the shaft
J	polar mass moment of inertia
K	reserve factors
k	stiffness
l	unsupported shaft section length
m	mass
mat	material of a ply
N	discrete quantity
n	number of plies
P	power
q	number of possible orientations in the staking sequence
r	shaft radius
S	cross-section area of the shaft
s	in-plane shear strength of the ply
T	axial torque
u	displacement (complex or real)
x, **y**, **z**	coordinates
X, X'	tensile and compressive longitudinal strength of the ply
Y, Y'	tensile and compressive transverse strength of the ply
α	orientation of the ply
η	loss factor
κ	shear coefficient
ν	Poisson's ratio of the shaft
υ	distribution of the torsional modes
ρ	mass density of the shaft
ϕ	in-plane cross-section rotation
σ_{11}, σ_{22}, σ_{12}	in-plane stress of the ply (longitudinal, transverse and shear)
ϖ	natural frequency of the torsional modes
ω	natural frequency of the flexural modes
Ω	spin speed

Subscript

B−, B+,	lower and higher backward whirl speeds
b	bearing
buck	buckling
c	critical
dv	driveline
e	external
eq	equivalent
F−, F+	lower and higher forward whirl speeds
f	flexural modes
G	gear
i	internal
inf	inferior
m	medium
min	minimum
nom	nominal
n	number of sine modes
ply	laminate ply
s	shaft
sup	superior
T	tail rotor
t	torsional modes
th	threshold speed
str	strength

each type of fibre. The main design considerations in the case of composite laminate tubes are the axial stiffness and torsional resistance. In this particular case, the plies providing stiffness and resistance can be considered quasi independently [14, 15]. HM carbon fibres which have poor mechanical properties when exposed to compression loads in particular [16], can serve to maximise the axial stiffness. HR carbon fibres can be used to maximise the resistance to torsion loads.

The first part of this paper presents various design aspects such as the rotordynamics (flexural and torsional vibrations), torsional strength and torsional buckling. The GA is then presented. The last part presents a comparative study between HM and hybrid solutions on a helicopter tail rotor driveline presented in the literature.

2. Design aspects

2.1. Rotordynamic analysis

When designing supercritical shafts, it is necessary to maximise the external damping in order to reduce the flexural imbalance responses and to increase the stability in the supercritical regime. There exist several techniques for increasing this non-rotating damping in a passive way. Most turbines use hydrodynamic bearings or squeeze-film dampers, but they have disadvantages such as the cost, the complexity of the system and the additional instabilities introduced

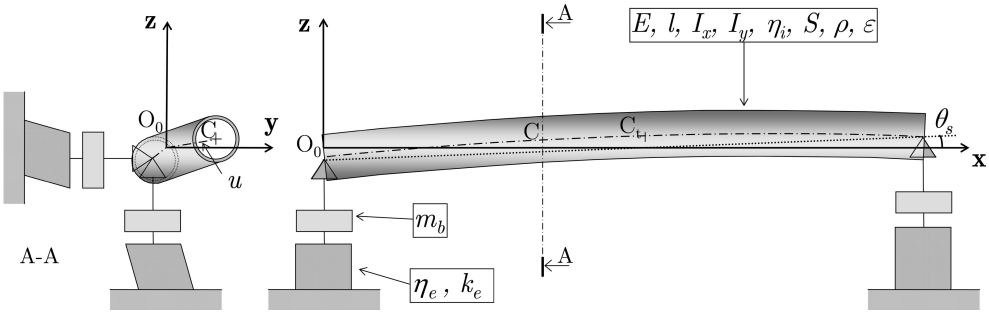

Figure 1: A simply supported axisymmetric tubular composite shaft with rolling-element bearings mounted on viscoelastic supports

; whereas rolling-element bearings do not destabilise rotors but provide insufficient damping. However, dissipative materials such as elastomers have recently emerged as suitable materials for bearing supports [17, 18, 19]. A corresponding low cost configuration, consisting of an axisymmetric composite shaft simply supported on classical rolling-element bearings mounted on viscoelastic materials, is investigated here (Fig. 1).

Various approaches based on beam and shell theories have been used to compute the flexural critical speeds of an axisymmetric tubular composite shaft mounted on elastic or infinitely rigid supports [20, 21, 22, 23]. The simplest of these approaches is called the Equivalent Modulus Beam Theory (EMBT) [1]. It is proposed here to use EMBT in the equations of motion previously studied in [18]:

$$\ddot{u} - \frac{I_y}{S}\left(1+\frac{E}{\kappa G}\right)\ddot{u_s}'' + \mathrm{i}\Omega\frac{I_x}{S}\dot{u_\mathrm{s}}'' + \frac{EI_y}{\rho S}u_\mathrm{s}'''' + \frac{c_i}{\rho S l}\left(\dot{u}_s - \mathrm{i}\Omega u_s\right) = 0 \tag{1}$$

where $u = u_y + \mathrm{i}u_z$ and $u_\mathrm{b} = u_{\mathrm{b}y} + \mathrm{i}u_{\mathrm{b}z}$ are the cross-sectional displacement and the deflection of the shaft respectively (see the list of nomenclature for other quantities). The above equation contains an additional term $\frac{E}{\kappa G}$ in comparison with the equation studied in [18]: it characterizes the effects of the transverse shear.

The above equation yields the four critical speeds for the nth harmonic (for details of the procedure, see [18]):

$$\omega_{\mathrm{c}n\mathrm{F}\pm} = \frac{1}{\sqrt{2\Delta_{n-}}}\left[\omega_{\mathrm{s}n}^2 + \Lambda_{n-}\omega_{\mathrm{b}n}^2 \pm \sqrt{\omega_{\mathrm{s}n}^4 + 2(\Lambda_{n-} - 2\Delta_{n-})\omega_{\mathrm{s}n}^2\omega_{\mathrm{b}n}^2 + \Lambda_{n-}^2\omega_{\mathrm{b}n}^4}\right]^{\frac{1}{2}} \tag{2}$$

$$\omega_{\mathrm{c}n\mathrm{B}\pm} = -\frac{1}{\sqrt{2\Delta_{n+}}}\left[\omega_{\mathrm{s}n}^2 + \Lambda_{n+}\omega_{\mathrm{b}n}^2 \pm \sqrt{\omega_{\mathrm{s}n}^4 + 2(\Lambda_{n+} - 2\Delta_{n+})\omega_{\mathrm{s}n}^2\omega_{\mathrm{b}n}^2 + \Lambda_{n+}^2\omega_{\mathrm{b}n}^4}\right]^{\frac{1}{2}} \tag{3}$$

with

$$\omega_{\mathrm{s}n}^2 = \frac{n^4\pi^4 EI_y}{\rho S l^4} = \frac{k_{\mathrm{s}n}}{m_\mathrm{s}},\ \omega_{\mathrm{b}n}^2 = \frac{k_\mathrm{e}}{m_\mathrm{b} + \frac{m_\mathrm{s}}{2(2+(-1)^n)}},\ \Delta_{n\pm} = \Psi_n \pm \Gamma_n,$$
$$\Delta_{n\pm} = \Psi_n \pm \Gamma_n,\ \Gamma_n = \frac{n^2\pi^2 I_x}{Sl^2},\ \Pi_n = 1 + \frac{n^2\pi^2 I_y}{Sl^2}\left(1+\frac{E}{\kappa G}\right),$$
$$\Phi_n = \frac{m_\mathrm{s}}{m_\mathrm{b} + \frac{m_\mathrm{s}}{2(2+(-1)^n)}},\ \Psi_n = \Pi_n - \frac{4}{n^2\pi^2}\Phi_n, \tag{4}$$

In addition in the case of a composite shaft consisting of a symmetric laminate, homogenised values (EMBT) have to be used : $E = 1/a_{11}e_\mathrm{s}$, $G = 1/a_{66}e_\mathrm{s}$, $\nu = -a_{12}/a_{11}$, $\kappa = 2(1+\nu)/(4+3\nu)$ and $\rho = m_\mathrm{s}/Sl$ where $\mathbf{a} = \mathbf{A}^{-1}$.

In the field of rotordynamics, internal damping, which is also referred as rotating damping, is known to cause whirl instability in the supercritical regime. In the literature, the internal damping resulting from dissipation in the shaft material and dry friction between the assembled components has been conventionally approached using the viscous damping model. However most materials have a vibratory damping, which resembles the hysteretic damping model much more than viscous damping, as in the case of carbon/epoxy materials [24, 25]. Based on a previous study using the classical equivalence between viscous and hysteretic damping [18], the analytical instability criterion suitable for the shaft optimisation can be written in the following form:

$$\pm\left(\eta_\mathrm{e}k_\mathrm{e}\Phi_n(\Pi_n\omega_{n\mathrm{F}\pm0}^2 - \omega_{\mathrm{s}n}^2) - \eta_\mathrm{i}k_{\mathrm{s}n}(\omega_{n\mathrm{F}\pm0}^2 - \omega_{\mathrm{b}n}^2)\right)$$
$$\begin{cases} < 0 & \Longrightarrow\ \omega_{\mathrm{th}\,n\mathrm{F}\pm} = \omega_{n\mathrm{F}\pm0} \\ \geqslant 0 & \Longrightarrow \text{stable} \end{cases} \tag{5}$$

where

$$\omega_{n\mathrm{F}\pm0} = \frac{1}{\sqrt{2\Psi_n}}\left[\omega_{\mathrm{s}n}^2 + \Pi_n\omega_{\mathrm{b}n}^2 \pm \sqrt{\omega_{\mathrm{s}n}^4 + 2(\Pi_n - 2\Psi_n)\omega_{\mathrm{s}n}^2\omega_{\mathrm{b}n}^2 + \Pi_n^2\omega_{\mathrm{b}n}^4}\right]^{\frac{1}{2}} \tag{6}$$

and where the equivalent longitudinal loss factor denoted η_i is computed with Adams, Bacon and Ni theory [26, 27] using complex properties of the ply (η_{11} =0.11 %, η_{22} =0.70 %

Table 1: Material properties corresponding to a volume fraction of 0.6

Material	Abbr.	ρ	E_{11}	E_{22}	E_{12}	X	X'	Y	Y'	S	e_{ply}
		kg m^{-3}	GPa	GPa	-	MPa	MPa	MPa	MPa	MPa	mm
Narmco 5505 [1]	BE[a]	1 965	211	24.1	0.36	1 365	1 586	45	213	62	0.1321
K63712/M10 [16]	HM	1 700	370	5.4	0.3	1 500	470	35	200	75	0.125
T800/G947	HR	1 530	162	10	0.3	2 940	1 570	60	290	100	0.125

[a] BE : boron/epoxy.

and η_{66} =1.10 %). It suffices then to compute the lowest threshold speed to determine the spin speed limit of the shaft.

2.2. Torsional vibration analysis

Assuming that the cross sections remain plane and radii of these cross sections remain straight, the classical torsional vibration equation is:

$$\rho I_x \ddot{\phi} = G I_x \phi'' \tag{7}$$

where ϕ and G are the twist angle at any cross section and the shear modulus, respectively. The natural torsional frequencies of the shaft are mainly due to the difference between the mass moment of inertia of the main gearing J_{G} and that of the tail rotor J_{T}. This assumption gives the boundary conditions:

$$J_{\text{G}} \ddot{\phi}(0,t) = G I_x \phi'(0,t) \tag{8}$$

$$J_{\text{T}} \ddot{\phi}(l,t) = -G I_x \phi'(l,t) \tag{9}$$

For the tail rotor drive shaft, it can be assumed that the polar mass moment of inertia of the shaft $J_{\text{s}} (= I_x \rho l)$ is small in comparison with that of the main gear and the tail rotor. The natural torsional frequencies can therefore be obtained directly from Eqs. (7-9) with an equivalent method of that used by Lim and Darlow [3]:

$$\bar{\omega}_n = \frac{v_n}{l}\sqrt{\frac{G}{\rho}} \quad \forall n \in \mathbb{N}^* \tag{10}$$

with

$$v_1 \approx \sqrt{2}\sqrt{\frac{J_{\text{G}}J_{\text{s}} + J_{\text{T}}J_{\text{s}} + J_{\text{s}}^2}{J_{\text{G}}J_{\text{s}} + J_{\text{T}}J_{\text{s}} + 2J_{\text{G}}J_{\text{T}}}},$$

$$v_{n\neq 1} \approx \frac{(n-1)\pi}{2} + \sqrt{\frac{(n-1)^2\pi^2}{4} + \frac{J_{\text{s}}}{J_{\text{T}}} + \frac{J_{\text{s}}}{J_{\text{G}}}} \tag{11}$$

2.3. Failure strength analysis

Only the torsional resistance of the shaft is considered. The transmitted torque causes only in-plane shear, which can be computed with classical laminate theory [28]. Contrary to an unsymmetrical free edge laminate plate, the tubular structure blocks the coupling effects in the case of small displacements. This can be modelled simply by assuming the classical coupling matrix **B** to be null before the inversion procedure required to compute the strain state.

A conservative approach in the case of helicopter drive shaft consists in computing only the fracture of the first ply. Classically, the Tsai-Wu criterion [29] can be used to account for differences between the tensile and compressive strength, which can be of great importance in the case of HM fibres (see Table 1):

$$\frac{1}{XX'}\sigma_{11}^2 + 2\frac{F_{12}}{\sqrt{XX'YY'}}\sigma_{11}\sigma_{22} + \frac{1}{YY'}\sigma_{22}^2 + \frac{1}{S^2}\sigma_{12}^2 + (\frac{1}{X} - \frac{1}{X'})\sigma_{11} + (\frac{1}{Y} - \frac{1}{Y'})\sigma_{22} \leq 1 \tag{12}$$

where F_{12} is an interaction parameter which is taken to be equal to 0.5. It should be noted that the Tsai-Wu criterion includes the transverse fracture mechanism. In the HR material, the transverse failure strain is approximately equal to 0.6 % while the longitudinal one is equal to 1.8 %. This type of fracture generally has no direct effects on the fracture of the laminate, and this approach seems to be too conservative. Assuming that the structure will be safe up to the occurrence of the first longitudinal or shear failure, we can obtain a more realistic torque resistance limit [15, 30]. This limit can be computed quite simply with a maximum stress criterion

$$-X' \leq \sigma_{11} \leq X \quad ; \quad |\sigma_{12}| \leq S \tag{13}$$

Comparisons between various criteria and experimental data are shown in Table 2. The tubes are prevent from buckling by taking a small length to diameter ratio. Tubes N°1 and 3 shown the value of assuming presence of a null coupling mechanism in the case of unsymmetrical laminates. The maximum stress criterion is in better agreement with the experimental data than the Tsai-Wu criterion. The Tsai-Wu estimation is improved by taking a double value for the tensile transverse resistance Y. Symmetric tube N°2 is in the pure shear state. All the criteria are equivalent in this case.

We previously described [16] the highly non-linear compressive behaviour of pitch-based fibres. The compressive modulus decreases dramatically which cannot be directly modelled with a linear criterion such as the above criteria. If the optimised solution includes +45° and/or -45° HM fibres plies, it will normally be necessary to improve the strength calculations. As we will see below, this will in fact not be necessary in the present case.

Table 2: Comparison between torque resistance calculations on various short boron/epoxy tubes

N°		1	2	3
Stacking sequence (from inner to outer radius)	°	[90,45,-45,90]	[90,0_2,90]	[90,45,-45,0_6,90]
Outer radius × length	mm	25.4 ×50.8	25.4×50.8	63.5×305
Experimental [1]	N.m	581	132	4689[a]
Tsai-Wu criterion	N.m	167 (-71%)	130 (3%)	1605 (-66%)
Tsai-Wu criterion with $\mathbf{B} = \mathbf{0}$	N.m	313 (-46%)	130 (3%)	2613 (-44%)
Tsai-Wu criterion with $Y \times 2$	N.m	285 (-50%)	130 (3%)	1608 (-66%)
Tsai-Wu criterion with $\mathbf{B} = \mathbf{0}$ and $Y \times 2$	N.m	496 (-14%)	130 (3%)	4138 (-12%)
Maximum stress in fibre and shear directions	N.m	517 (-10%)	130 (3%)	1610 (-66%)
Maximum stress in fibre and shear directions with $\mathbf{B} = \mathbf{0}$	N.m	585 (2%)	130 (3%)	4880 (4%)
Buckling computed with Hayashi [31] criterion	N.m	1049	1547	13 016

[a] Mean value of two specimen tests.

2.4. Torsional buckling analysis

The finite element method is the most frequently employed method of computing torsional buckling. However, it is suitable here a method requiring less computing time. The other possibility consists in solving the buckling shell theory in the case of orthotropic circular cylinders. Assuming that we have a symmetric laminate and a sufficiently long shaft, some criteria deduced from shell theory can be obtained, in particular that of Hayashi [31]

$$T_{\text{buck}} = 11\sqrt{r_{\text{m}}}\left(A_{11} - \frac{A_{12}^2}{A_{22}}\right)^{1/4} D_{22}^{3/4} \tag{14}$$

where r_{m} is the medium radius of the shaft, and A_{11}, A_{22}, A_{12} and D_{22} are homogenised moduli of the laminate. Shell theory is used here to account for the unsymmetrical laminate. Laminate theory is included in Flügge's shell equations [32, 33]. Assuming that we are dealing with a long cylinder, we can solve the shell equations with the simplified displacement field proposed by Flügge [32]. In mathematical terms, the torque is obtained numerically by minimising a 3×3 determinant. These two methods of modelling and the finite element method for shells are compared on unsymmetrical stacking sequence in Table 3. All the tubes have the same size and the laminate all have the same thickness. Buckling torque is computed in the positive and then in the negative direction. The results obtained with the finite element method using ABAQUS (s4 elements) [34], which were previously validated based on experimental results obtained by Bauchau et al. [35] in [25], are taken as reference values. The table shows that the Hayashi criterion overestimates the buckling torque, especially in the largest unsymmetrical laminates (N°9-12) by up to 40%. The results obtained with Flügge theory on long tubes with laminate theory show good agreement with finite element calculation giving a conservative estimate on the whole. The largest errors amount to only 8% and the mean error is 4%. Note that the long tube assumption investigated in [25], is useful when the length-to-diameter ratio is greater than 100 and the diameter-to-thickness ratio is greater than 40.

2.5. Driveline mass

The driveline is composed of shafts and intermediate supports, which include bearings, fittings, and supports. The intermediate support mass m_{b} can be computed with an empirical equation from Lim and Darlow [3]

$$m_{\text{b}} = 17.1288\left(\frac{P_{\text{dv}}}{\Omega_{\text{nom}}}\right)^{0.69} \tag{15}$$

where P_{dv} is the power transmitted with the driveline (in W) and Ω_{nom} is the nominal spin speed (in rev / min). The driveline mass can then be computed using the following expression:

$$m_{\text{dv}} = N_{\text{s}} \times m_{\text{s}} + N_{\text{b}} \times m_{\text{b}} \quad \text{with} \quad m_{\text{s}} = \rho S l \tag{16}$$

where N_{s} is the number of shafts and N_{b} is the number of intermediate supports.

3. Shaft optimisation using a genetic algorithm

The principle of the GA algorithm is the same as that on which Darwin's theory of evolution is based. At the beginning, a population is randomly created and evaluated with a fitness function. This evaluation gives the adaptability of each individual. Starting with this information, the whole population can be evolved using selection, crossover and mutation operators. This process is iterated up to convergence.

The main risk of this stochastic method is that of not obtaining the optimum solution. In particular, GA may tend to converge on local optima and may not be able to cross these attracting points. Another weakness of the method is the large amount of fitness function calculations required. This means that the evaluation procedure must not be very time-consuming.

3.1. Individual

An individual in this driveline optimisation procedure consists of the medium diameter r_{m} (which can be fixed or otherwise), the bearing stiffness k_{e} (fixed or not), the nominal spin speed Ω_{nom} and the stacking sequence with various materials, symmetric or not, as in the following example : $[\alpha_1^{\text{mat}_1} \times$

Table 3: Buckling torque of carbon/epoxy laminate tubes: comparison between methods of computation (l = 4 m, r_m = 40 mm, E_{11} = 134 GPa, E_{22} = 8.5 GPa, $E_{66} = E_{55}$ = 4.6GPa, E_{44} = 4.0 GPa, E_{12} = 0.29, e_s = 1.067 mm)

Laminate		ABAQUS		Flügge with laminate theory		Hayashi criterion	
N°		Mesh[a]	Nm	Nm	%	Nm	%
1	$[15,-15]_4$	60-150	210	193	-8	222	6
2	$[-15,15]_4$	60-150	214	197	-8	222	4
3	$[30,-30]_4$	60-150	263	254	-4	283	8
4	$[-30,30]_4$	60-150	268	259	-3	283	6
5	$[45,-45]_4$	60-150	385	383	-1	419	9
6	$[-45,45]_4$	60-150	385	382	-1	419	9
7	$[0_2,45,-45,45,-45,0_2]$	60-150	230	218	-5	252	10
8	$[0_2,-45,45,-45,45,0_2]$	60-150	219	208	-5	252	15
9	$[0_2,45,0,-45,0,45,-45]$	30-100	358	342	-4	420	17
10	$[0_2,-45,0,45,0,-45,45]$	30-100	329	315	-4	420	28
11	$[0_2,45,0_2,-45,45,-45]$	30-100	355	340	-4	440	24
12	$[0_2,-45,0_2,45,-45,45]$	30-100	313	300	-4	440	41
13	[-45,-15,15,45,15,-15,-45,45]	60-150	389	375	-4	493	27
14	[45,15,-15,-45,-15,15,45,-45]	60-150	439	449	2	493	12
15	[15,-15,-45,-15,15,45,15,-15]	60-150	219	206	-6	265	21
16	[-15,15,45,15,-15,-45,-15,15]	60-150	241	226	-6	265	10

[a] Number of circumferential elements - number of lengthwise elements.

$n_1, ..., \alpha_j^{\mathrm{mat}_j} \times n_j, ..., \alpha_q^{\mathrm{mat}_q} \times n_q]$ where α_j , n_j and mat_j are the orientation, the quantity and the material of the ply j, respectively. Under supercritical conditions, the bearing stiffness is a necessary optimisation variable because it appears in the rigid mode frequencies Eq. (4) and the stability criterion Eq. (5). The shaft length corresponds to the driveline length divided by the number of shafts.

There are several possible ways of modelling the chromosomes of individuals. It is proposed here to fix the number of possible orientations in the stacking sequence, denoted q. This sets the size of the chromosome for a particular optimisation which simplifies the crossover operations. Individuals are classically represented by an array of binary numbers. The orientation α_j can be written with 2, 3 or 4 bits to stand for the sets {-45, 0, 45, 90}, {-67.5, -45, -22.5, 0, 22.5, 45, 67.5, 90} or {-75, -60, -45, -30, 15, 0, 15, 30, 45, 60, 75, 90, 105, 120, 135, 150} (in degree units), respectively, which correspond to realistic manufacturing orientations. The quantity n_j is written with 2 or 3 bits corresponding to the sets {1,2,3,4} and {1,2,3,4,5,6,7,8}, respectively. The material mat_j is written with one bit to take the advantage of both HM and HR carbon fibres, or metal and HM carbon fibres, for example. Lastly, k_e and r_m are bounded and generally encoded with 3 bits. For example, a shaft with the following stacking sequence $[45_2^{\mathrm{mat}_1}, 0_3^{\mathrm{mat}_2}]$ (i.e. $q = 2$), with r_m =52 mm and Ω_{nom} =4000 rev/min, with the bearing stiffness fixed and where α_j and n_j are encoded with 2 bits, r_m with 4 bits, Ω_{nom} with 3 bits and mat_j with 1 bit, is defined by the following chromosome:

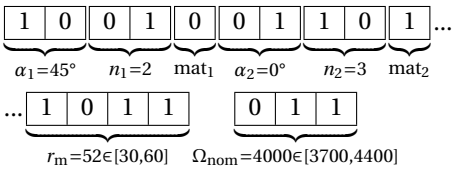

The string length is therefore simply $(\mathrm{bit}_\alpha + \mathrm{bit}_n + \mathrm{bit}_{\mathrm{mat}}) \times q + \mathrm{bit}_{k_e} + \mathrm{bit}_{r_m} + \mathrm{bit}_{\Omega_{nom}}$.

3.2. Constraints and fitness

The mass is the optimised value generally used in driveline problems [3, 6, 36]. In this paper, a part of the fitness function is inversely proportional to the mass of one shaft. The fitness function depends also on the resistance, buckling and dynamic constraints previously investigated ($n \in \mathbb{N}^*$):

$$g_1 = \frac{K_{\mathrm{str}} T_{\mathrm{str}}}{T_{\mathrm{nom}}} - 1 \geq 0 \quad \text{with} \quad K_{\mathrm{str}} \leq 1 \tag{17}$$

$$g_2 = \frac{K_{\mathrm{buck}} T_{\mathrm{buck}}}{T_{\mathrm{nom}}} - 1 \geq 0 \quad \text{with} \quad K_{\mathrm{buck}} \leq 1 \tag{18}$$

$$g_3 = \frac{e_s}{e_{s\min}} - 1 \geq 0 \tag{19}$$

$$g_{4n} = 1 - \frac{K_{\mathrm{tinf}\,n} \Omega_n}{\Omega_{\mathrm{nom}}} \geq 0 \quad \text{with} \quad K_{\mathrm{tinf}\,n} \geq 1 \tag{20}$$

$$g_{5n} = \frac{K_{\mathrm{tsup}\,n} \Omega_n}{\Omega_{\mathrm{nom}}} - 1 \geq 0 \quad \text{with} \quad K_{\mathrm{tsup}\,n} \leq 1 \tag{21}$$

and in the subcritical case

$$g_6 = \frac{K_{\mathrm{fsup}\,1} \omega_{c1}}{\Omega_{\mathrm{nom}}} - 1 > 0 \quad \text{with} \quad K_{\mathrm{fsup}\,1} \leq 1 \tag{22}$$

or in the supercritical case

$$g_{7n} = 1 - \frac{K_{\text{finf}\,n}\omega_{cn}}{\Omega_{\text{nom}}} \geq 0 \quad \text{with} \quad K_{\text{finf}\,n} \geq 1 \tag{23}$$

$$g_{8n} = \frac{K_{\text{fsup}\,n}\omega_{cn}}{\Omega_{\text{nom}}} - 1 \geq 0 \quad \text{with} \quad K_{\text{fsup}\,n} \leq 1 \tag{24}$$

$$g_9 = \frac{K_{\text{th}}\omega_{\text{th}}}{\Omega_{\text{nom}}} - 1 \geq 0 \quad \text{with} \quad K_{\text{th}} \leq 1 \tag{25}$$

where g_i and $K_{...}$ are constraint functions and reserve factors, respectively. Eq. (17) corresponds to the torsional strength constraint, which requires that the torque computed with the resistance criterion multiplied by the reserve factor is smaller than the torque required. Eq. (18) is used here for the torsional buckling. The other equations are those giving the dynamic constraints. Eqs. (20-21) correspond to the positioning of the nominal spin speed between torsional modal frequencies. Regarding the bending modes, the constraints depend on which of the two cases applies: the subcritical or supercritical case. In the first case, Eq. (22) corresponds to the subcritical assumption, i.e. the nominal spin speed multiplied by the reserve factor must be smaller than the first critical speed. In the supercritical case, Eqs. (23-24) correspond to the positioning of the nominal spin speed between the flexural critical speeds, and Eq. (25) corresponds to the stability constraint.

GAs can not account directly of constraint functions. This problem can be overcome by using a penalisation method consisting in deteriorating the quality of an individual that violate one or more constraints by decreasing the fitness function. The fitness function for mass minimisation can be written in the general following form

$$f = \frac{1}{m_{\text{s}}} + \sum_j \gamma_j \min(0, g_j) \tag{26}$$

where γ_j are the penalisation factors. The reserve factors and penalisation factors are given in Table 4.

3.3. The genetic algorithm method

3.3.1. Initialisation

The algorithm is initialised by randomly generating a population of 300-600 individuals. The number depends on the size of the problem.

3.3.2. Elitism

After evaluating the population with the fitness function, the two fittest individuals, also called the elites, are selected and kept for the next generation.

3.3.3. Scaling, selection and crossover

With the progression of the GA, the fitness of all the individuals tends to converge on that of the fittest ones. This decelerates the progress of the algorithm. In order to overcome this problem, scaling methods such as windowing, exponential, linear transformation or linear normalisation methods can be used [7]. A windowing method is used here, whereby the fitness of the lowest ranking individual is subtracted from the fitness of each individual. Two parents are then selected, based on their scaled fitness values and a multi-point crossover operation is performed. The cutting point is selected randomly. This operation gives two children, forming the next generation. Note that elites can be parents.

Table 5: Search parameters of the genetic algorithm

Population size	300-600
Chromosome length	24-34
Crossover probability	90%
Mutation probability	10%
Number of generation	150-40000

3.3.4. Mutation

The mutation operation consists in randomly modifying the bits of the chromosomes. The probability of the mutation must be very high to obtain a highly diverse population. But if the mutation process is too strong, the algorithm may not converge on the optimum fitness. Note that elites are not subject to mutation operations. After the mutation, the process is restarted at the elitism stage until the maximum fitness function is reached.

The search parameters of the GA are given in Table 5.

4. Case study

A helicopter tail rotor driveline presented by Zinberg and Symonds [1] is investigated with the GA. The original driveline with a total length of 7.41 m, which is assumed to transmit a power of 447.4 kW, is composed of five subcritical aluminium alloy tubes and four intermediate supports. Zinberg and Symonds proposed to replace the conventional driveline by three subcritical composite shafts consisting of boron/epoxy material. The properties of this composite shaft can be compared with those of the aluminium one in Table 6. Note that the Zinberg shaft was obtained only on the basis of physical considerations.

In line with Lim and Darlow [3] who studied the same driveline case, the mass moment of inertia of the main gearing and tail rotor were assumed to be equal to 0.94 kg m^2 and 3.76 kg m^2, respectively. To take the difference between the connections in the metallic and composite shafts into account, a weight penalty of 1.5 kg per composite shaft is added here.

4.1. Subcritical shaft optimisation

Subcritical shaft optimisation was first studied with the GA. The case of two single-materials (boron/epoxy and HM/epoxy) and one hybrid case (HR/HM) was examinated (see Table 1 for the properties of the materials). The optimisation was computed six times with each material to check that convergence of the GA was reached. The results of the optimisation are shown in Fig. 2 and the properties of the fittest individuals are summarise in Table 6 in each case. Figs. 2a-2d show the fitness function of the highest ranking individual during

Table 4: Reserve factors and penalisation factors

K_{tsai}	K_{buck}	$K_{\text{tsup}\,n}$	$K_{\text{tinf}\,n}$	$K_{\text{fsup}\,n}$	$K_{\text{finf}\,n}$	K_{th}	$\gamma_{1,2}$	γ_3	$\gamma_{j\notin\{1,2,3\}}$
0.44	0.44	0.83	1.15	0.8	1.2	0.8	2	6	4

Table 6: Optimised boron and carbon/epoxy tail rotor driveline under subcritical conditions in comparison with the conventional aluminium tail rotor driveline

			Conv.	Zinberg	Optimised			
Material			aluminium	BE[1]	BE	HM	HM^b	HR/HM
Number of tubes		-	5			3		
String length		bit	-	-	24	24	30	30
Stacking sequence (from inner to outer radius)		°	-	[90,45, -45,0_6, 90]	[90_2,0_4, -45,45, 90]	[90,0_3, 45,-45_2, 45]	[90,-22.5_2, 22.5,-22.5, 22.5_2,-67.5]	[90^{HM},45^{HR}, 0_4^{HM},-45^{HR}, 90^{HM}]
Operating speed	Ω_{nom}	rev / min	5 540	4 320	3 800	4 800	4 600	4 400
1st critical speed	ω_1	rev / min	8 887	5 697^a	4 606	5 800	5 695	5344
1st torsion mode	ϖ_1	rev / min	2 058^a	1 292^a	1 065	1 534	1 254	635
2nd torsion mode	ϖ_2	rev / min	65 370^a	35 318^a	36 428	64 965	59 599	34 510
Nominal torque	T_{nom}	N m	771	989	1 124	891	929	971
Strength torque	T_{str}	N m	4 925^a	4 880 ^{a}	3 149	2 268	2 267	3 349
Buckling torque	T_{buck}	N m	3 090^a	2 671^a	2 645	2 108	2 105	2 206
Tube length	l	m	1.482			2.470		
Mean tube radius	r_{m}	mm	56.3	62.84	56	54	50	46
Tube thickness	e_{s}	mm	1.65	1.321	1.19	1.00	1.00	1.00
Tubes weight	$N_{\text{s}}m_{\text{s}}$	kg (%)	13.38	8.16 (61)	6.09 (46)	4.26 (32)	3.96 (30)	3.57 (27)
Supports weight	$N_{\text{b}}m_{\text{b}}$	kg	15.42	7.71	9.68	8.24	8.48	8.75
Weight penalty		kg	-	4.5^a	4.5	4.5	4.5	4.5
Total weight	m_{dv}	kg	28.80	20.37^a	20.27	17	16.95	16.82
Weight saving		kg (%)	-	8.4 (29)^a	8.5 (30)	11.8 (41)	11.9 (41)	12.0 (42)

^{a} Value computed with presented methods. ^{b} with $\text{bit}_\alpha = 3$

the evolution (number of generations) in six different populations. The legend gives the properties of the fittest individual in each population at the last generation. The results obtained show that the five conventional shafts can be replaced by three subcritical boron or carbon/epoxy shafts. The algorithm did not find any subcritical solutions with only two shafts. We noted that operating speed was much higher than the first natural torsional frequency in all the solutions.

In the boron/epoxy case (Fig. 2a), GA yielded three different solutions with the same fitness after 2000 generations. All the solutions gave the same radius, the same operating speed and the same plies (three 90° plies, four 0° plies, one -45° ply and one 45° ply) but various stacking sequence orders. They also gave the same critical speeds and the same resistance. The independence of critical speed computations from the stacking sequence order is due to EMBT. As far as the resistance is concerned, this independence results from in-plane shear loading and the assumption that uncoupled tension-bending is involved ($\mathbf{B} = \mathbf{0}$). On the other hand, torsional buckling is dependent of the stacking sequence order, as shown in Table 3. In particular, the circumferential flexural stiffness of the laminate is highly significant. This explains the position of the 90°plies, which are located in the inner and outer parts of the tube. The solution with the greatest buckling torque was selected as the best individual. The stacking sequence obtained ([$90°_2$, $0°_4$, 45°, -45°, 90°]) is very similar to that of Zinberg and Symonds' laminate ([90°, 45°, -45°, $0°_6$, 90°]), only two 0° plies were replaced by a 90° ply. The decrease in the shaft thickness and shaft radius explain the slight increase in weight saving from 29% to 30% obtained in comparison with the conventional aluminium shaft (see Table 6). The computing time required for one evolution was approximately equal to 50 minutes using MATLAB [37] on a Xeon E5540.

The second material tested was HM carbon/epoxy (Fig. 2b). Convergence was reached after 200 generations, but five different solutions were obtained with the same fitness. Only the order between 0°, 45° and -45° plies and the operating speed were different. The optimum shaft stacking sequence maximising the resistance and buckling margins was [90°, $0°_3$, 45°, $-45°_2$, 45°]. This gave the minimum thickness authorized (1 mm). Due to the high level of stiffness in comparison with boron/epoxy, only one 90° ply was necessary to prevent buckling and three 0° plies were required to avoid reaching the first critical speed. The number of ±45° plies was doubled due to the low resistance of HM carbon/epoxy. The weight saving increased considerably in comparison with the previous example, reaching 41% due to several combined effects: the de-

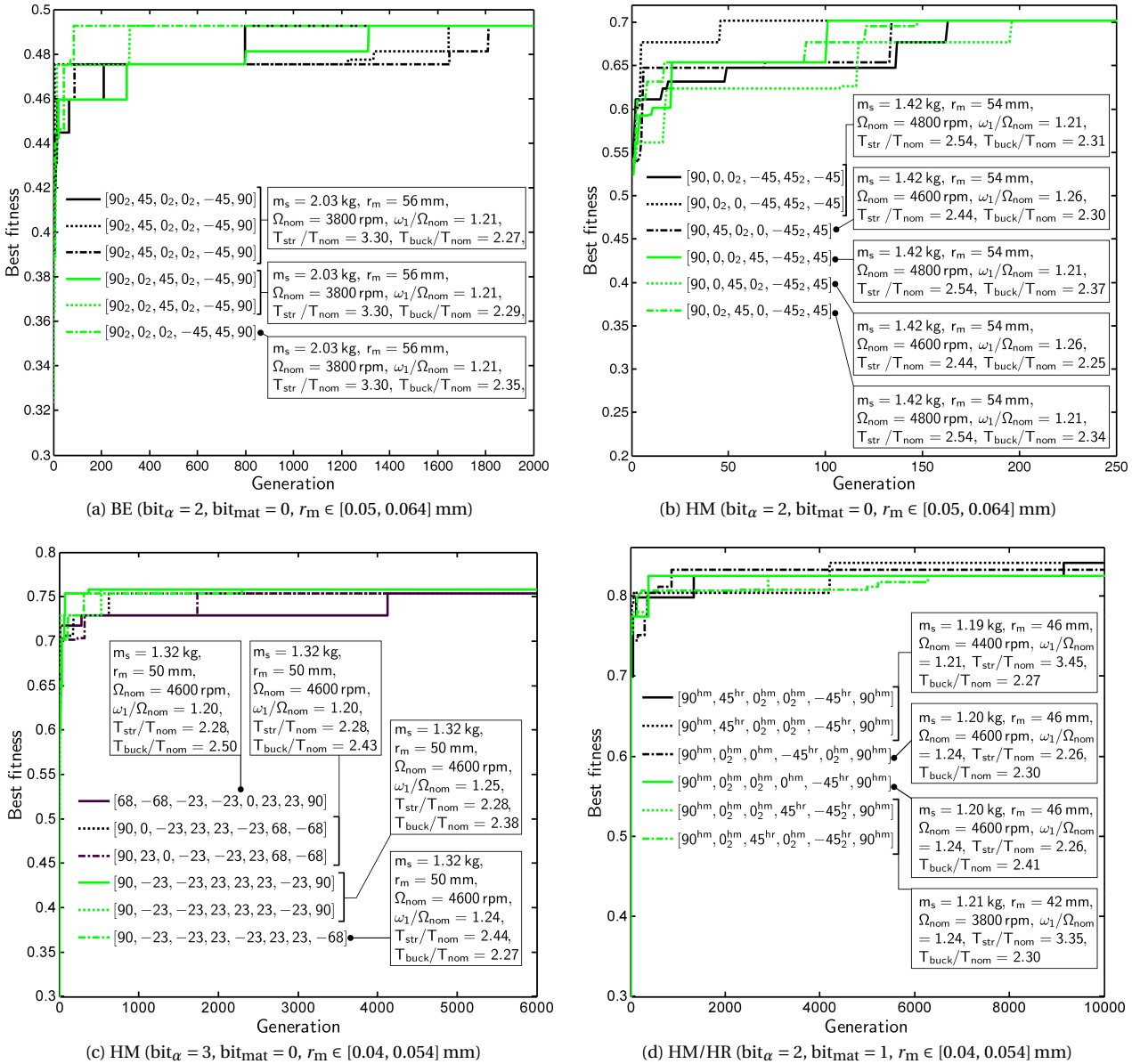

(a) BE ($\text{bit}_\alpha = 2$, $\text{bit}_{\text{mat}} = 0$, $r_{\text{m}} \in [0.05, 0.064]$ mm)

(b) HM ($\text{bit}_\alpha = 2$, $\text{bit}_{\text{mat}} = 0$, $r_{\text{m}} \in [0.05, 0.064]$ mm)

(c) HM ($\text{bit}_\alpha = 3$, $\text{bit}_{\text{mat}} = 0$, $r_{\text{m}} \in [0.04, 0.054]$ mm)

(d) HM/HR ($\text{bit}_\alpha = 2$, $\text{bit}_{\text{mat}} = 1$, $r_{\text{m}} \in [0.04, 0.054]$ mm)

Figure 2: Evolution of the best individual fitness of several shaft populations in the case of various materials, subcritical conditions and three tubes forming the Zinberg and Symonds tail rotor driveline (there were 300 individuals in each evolution with $\text{bit}_n = 1$, $\text{bit}_{r_{\text{m}}} = 3$, $\text{bit}_{\Omega_{\text{nom}}} = 3$, $q = 6$, $\Omega_{\text{nom}} \in [3800, 5200]$ rev / min, $e_{\text{s}\min} = 1$ mm and l =2.470 m)

crease in the density, the mean tube radius, the thickness and the weight of the supports (due to the increase in the operating speed, see Eq. (15)).

The optimisation of the HM material was then carried out with $\text{bit}_\alpha = 3$ i.e. $\alpha \in$ {-67.5°, -45°, -22.5°, 0°, 22.5°, 45°, 67.5°, 90°} (Fig. 2c). The chromosome length increased from 24 to 30. This considerably increased the search-space, and hence the number of generations required to obtain convergence and the computing time (approximately 3h/evolution). Convergence was obtained after approximately 6000 generations. Four different optimum individuals were obtained with the same fitness. All of them contained (+ and -)22.5° plies and most of them contained (+ and/or -)67.5° plies. The optimum shaft selected from four solutions was [90°,-23°$_2$,23°,-23°,23°$_2$,-68°]. This shaft did not contain 0° plies and can be manufactured with a filament winding process. The weight saving increased slightly in comparison with the previous case due to the decrease in the mean tube radius.

The last case tested was the hybrid HR/HM case (Fig. 2d). Convergence was again obtained after approximately 6000 generations, despite the fact that only three evolutions yielded the optimum individual. The optimum stacking sequence obtained was [90°$^{\text{HM}}$, 45°$^{\text{HR}}$, 0°$^{\text{HM}}_4$, -45°$^{\text{HR}}$, 90°$^{\text{HM}}$]. These results require some simple comments. The 90° and 0° plies consisted of HM fibres because these plies determine the stiffness problems (the dynamics and buckling). The ±45° plies

consisted of HR fibres because these plies determine the strength problem. The weight reduction in comparison with the HM case was lower than expected. In fact, the decrease in the shaft weight was practically balanced by the increase in the weight of the supports.

The optimisation procedure was also carried out in the case of HR material (results not presented here). In the configuration studied here, HR material gave a fitness in between that obtained in the case of BE and HM material, due to its low density.

In addition, it is worth noting that the number of generations required to converge on the global optimum depended on the size of the search-space, as well as on the basin of attraction of the local and global optima. For example in the case of two materials with the same chromosome length, the number of generations required to reach convergence increased from 250 to 2000 (Figs. 2a-2b).

4.2. Supercritical shaft optimisation

In this part, the subcritical condition was removed. The optimisation was performed in the case of one single-material (HM) and one hybrid material (HR/HM). The results obtained show that the five conventional shafts can be replaced by either one or two supercritical shafts (see Table 7 and Figs. 3-4). Contrary to the subcritical optimisation, it is necessary here to take the first four critical speeds and the threshold speed into account. The support stiffness was used as a supplementary optimisation variable to maximise the dynamic stability margin. Lim and Darlow [3] proposed to optimise one shaft case with a carbon/epoxy material denoted here CE_L (Table 1). These authors used a generalised reduced gradient method that imposed continuous variables such as the fraction and the orientation of the laminate plies. Among the stacking sequences tested, $[0°_{\alpha}, \phi_{\beta p}, -\phi_{\beta n}, 90°_{\gamma}]_s$, the optimum one was $[0°_{64\%}, -62°_{4\%}, 90°_{32\%}]_s$ (Table 7). The operating speed was above the third critical speed and the dynamic stability was not taken into account.

In the two-tube case, the first material studied was HM carbon/epoxy (Fig. 3a). Convergence was reached with three populations after approximately 6 000 generations. The stacking sequence of the optimum shaft (involving larger margins) was [90°, 45°, $0°_2$, $-45°_2$, 0°, 45°]. This sequence is the same as in the subcritical case, only the order is slightly different. The shaft radius increased from 54 to 56 mm. Note that in Fig. 3a, all the margins are particularly large (≥ 2). In particular, the operating speed was in between the first and second critical speeds, far above the threshold speed. Much greater weight saving was obtained than with the conventional aluminium shaft (61%) or optimum subcritical shaft. This was essentially due to the removal of one intermediate support.

The second case tested was that of the hybrid HM/HR material (Fig. 3b). Five populations converged onto the optimum fitness after 10 000 generations. All the stacking sequences consisted of five 0° plies in HM carbon, two 90° plies in HM carbon, and one (+ or -)45° ply in HR carbon. The fittest individual was [$90°^{HM}$, $0°_3^{HM}$, $-45°^{HR}$, $0°_2^{HM}$, $90°^{HM}$]. This outcome was similar to that obtained in the subcritical case, only one $45°^{HR}$ ply was replaced by one $0°^{HM}$ ply. The weight saving was greater than in the HM case and reaching 63%.

In the one-tube case, only hybrid HM/HR material was studied (Fig. 4). Convergence was reached with five populations after approximately 20 000 generations. The stacking sequence corresponding to the optimum individual was [$90°^{HR}$, $0°_9^{HM}$, $-45°^{HR}$]. It is worth noting that the number of 0° plies increases considerably in comparison with the two-tube case from 5 to 9, mainly due to the fact that the dynamic constraints were met. The operating speed here was in between the second and third critical speeds. The AG selected HR fibres for the 90° ply here instead of HM fibres, which was unusual, possibly because the tube thickness was larger than in the previous cases tested, which reduced the buckling risk. The weight saving here amounted to 72%, which is almost equal to that obtained by Lim and Darlow [3]. However, this solution is more efficient because the operating speed is above the second critical speed and the dynamic stability was ensured.

We carried out the above optimisation procedure with $bit_{\alpha} = 3$. After 40 000 generations with 8 populations of 600 individuals, AG did not find a better solution. In this case, the computing time increased dramatically, amounting to approximately 18 hours per population.

5. Conclusion

In the first part of this study, various models and criteria are presented for designing supercritical composite drive shafts. In particular, the following three points are worth noting. First, the dynamic analysis showed the destabilising effects of internal hysteretic damping in the supercritical region. It is therefore necessary to compute this effect to ensure the integrity of the system at the nominal speed. Secondly, the failure strength of composite tubes can be computed with the maximum stress criterion in the longitudinal and shear directions, assuming coupling effects to be null. The results obtained using this simplified approach show good agreement with the experimental data. Lastly, the torsional buckling classical criteria do not take the coupling mechanism involved in unsymmetrical laminates into account, and this can result in large errors in the buckling torque estimates. In this particular case, a laminate theory obtained with Flügge's shell equations and solved with Flügge's displacement field for long tubes gives a better approximation of the buckling torque.

In the second part of this study, a GA is presented for optimising applications of this kind. This method was tested on an example available in the literature and found to be valid. The computing time was quite reasonable, generally amounting to less than one day. This was possible only because analytic results and simple methods were used. On the other hand, the algorithm does not ensure convergence on a single optimum individual but yield several solutions with practically the same mass. This study also shows the efficiency of hybrid solutions based on high modulus/high resistance carbon fibres. In the example presented here, the hybrid solution

Table 7: Optimised carbon/epoxy tail rotor driveline under supercritical conditions in comparison with the conventional aluminium tail rotor driveline

Material			Conv. aluminium	Lim CE_L [3]	HM	HR/HM	HR/HM
Number of tubes		-	5	1	2	2	1
String length		bit	-	-	27	33	34
Stacking sequence (from inner to outer radius)		°	-	$[0_{64\%}, -62_{4\%}, 90_{32\%}]_s$	[90,45, 0_2,−45$_2$, 0,45]	[90^{HM},0_3^{HM}, -45^{HR},0_2^{HM}, 90^{HM}]	[90^{HR},0_9^{HM}, -45^{HR}]
Operating speed	Ω_{nom}	rev / min	5 540	6000	5 400	4 800	7 000
1st critical speed	ω_1	rev / min	8 887	490	2 696	2 647	1 018
2nd critical speed	ω_2	rev / min	-	1 913[a]	10 784	10 589	4 072
3nd critical speed	ω_3	rev / min	-	4 303[a]	24 264	23 824	9 161
4th critical speed	ω_4	rev / min	-	7 650[a]	43 136	42 355	16 287
1st torsion mode	$\bar{\omega}_1$	rev / min	2 058[a]	389[a]	1 322	409	483
2nd torsion mode	$\bar{\omega}_2$	rev / min	65 370[a]	8 846[a]	43 326	18 112	8 300
Threshold speed	ω_{th}	rev / min	-	-[b]	23 658	20 356	13 638
Nominal torque	T_{nom}	N m	771	712	791	891	610
Strength torque	T_{tsai}	N m	4 925[a]	1 492[a]	2 439	2 096	4 352
Buckling torque	T_{buck}	N m	3 090[a]	1 460[a]	1 963	2 137	1 657
Tube length	l	m	1.482	7.41	3.705	3.705	7.41
Mean tube radius	r_m	mm	56.3	47.7	56.0	50.0	62.0
Tube thickness	e_s	mm	1.65	1.69	1.0	1.0	1.375
Support stiffness	k_e	kN m^{-1}	-	-[b]	2 864	2 864	1 437
Tubes weight	$N_s m_s$	kg (%)	13.38	6.08 (45)	4.43 (33)	3.60 (27)	6.65 (50)
Supports weight	$N_b m_b$	kg	15.42	0	3.80	4.12	0
Weight penalty		kg	-	1.5	3.0	3.0	1.5
Total weight	m_{dv}	kg	28.80	7.58[a]	11.23	10.72	8.15
Weight saving		kg (%)	-	21.22 (74)	17.6 (61)	18.1 (63)	20.7 (72)

[a] Value computed with presented methods. [b] Not under consideration in the reference.

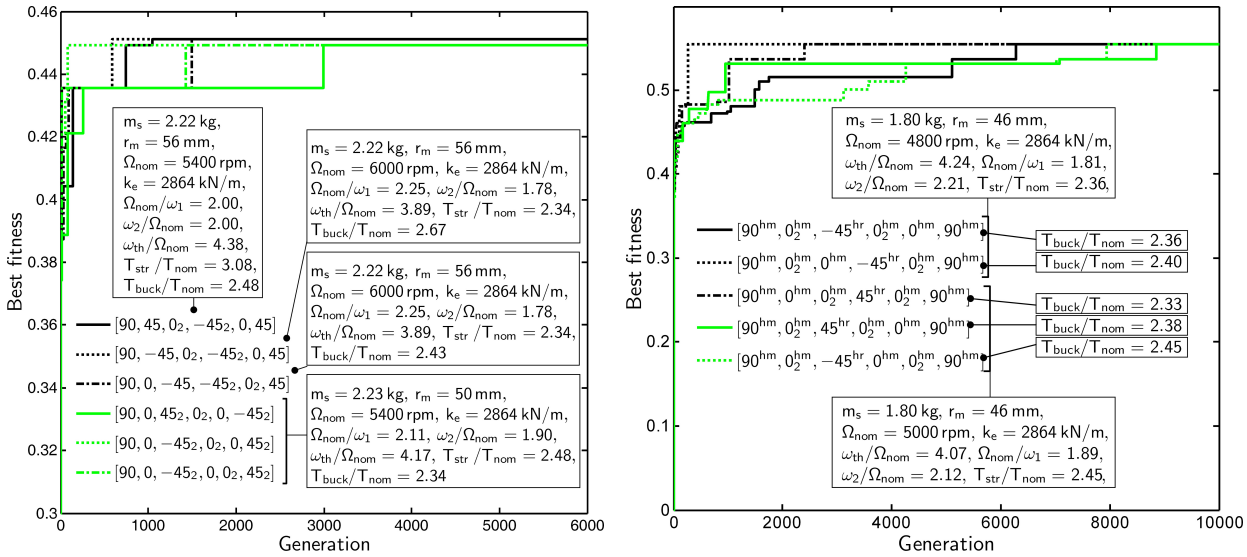

(a) HM ($bit_{mat} = 0$, $r_m \in [0.046, 0.06]$ mm, $\Omega_{nom} \in [4800, 6200]$ rev / min)

(b) HM/HR ($bit_{mat} = 1$, $r_m \in [0.046, 0.06]$ mm, $\Omega_{nom} \in [4800, 6200]$ rev / min)

Figure 3: Evolution of the best individual fitness of several shaft populations in the case of various materials, supercritical conditions and two tubes forming the Zinberg and Symonds tail rotor driveline (there were 300 individuals in each evolution with $bit_\alpha = 2$, $bit_n = 1$, $bit_{r_m} = 3$, $bit_{k_e} = 3$, $bit_{\Omega_{nom}} = 3$, $q = 6$, $k_e \in [10^4, 10^7]$ N m^{-1}, $e_{s\,min} = 1$ mm, $\eta_e = 0.1$ and l =3.705 m)

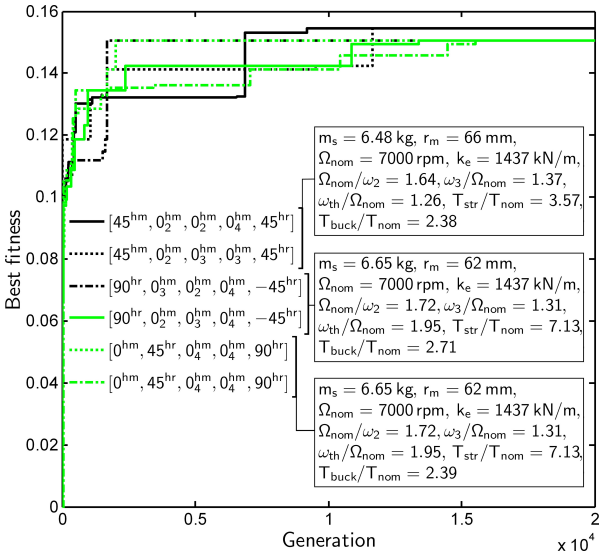

Figure 4: Evolution of the best individual fitness of several shaft populations in the case of HM/HR material, supercritical conditions and one tube forming the Zinberg and Symonds tail rotor driveline (there were 600 individuals in each evolution with $\text{bit}_\alpha = 2$, $\text{bit}_{\text{mat}} = 1$, $\text{bit}_n = 2$, $\text{bit}_{r_\text{m}} = 3$, $\text{bit}_{k_\text{e}} = 3$, $\text{bit}_{\Omega_\text{nom}} = 3$, $q = 5$, $r_\text{m} \in [0.052, 0.066]$ mm, $\Omega_\text{nom} \in [5600, 7000]$ rev / min, $k_\text{e} \in [10^4, 10^7]$ N m^{-1}, $e_{\text{s}\min} = 1$ mm, $\eta_\text{e} = 0.1$ and l =7.410 m)

made it possible to replace the conventional driveline consisting of five aluminium tubes by three subcritical composite shafts or a single supercritical composite shaft. The weight saving obtained was equal to 42% and 72%, respectively. The supercritical solution was found to be stable, operating above the second critical speed. In most of the cases studied, the algorithm confirmed the general rules, previously established without the use of an optimisation algorithm [38] for defining the stacking sequence of hybrid solutions:

1. ±45° HR carbon/epoxy plies should be used in order to maximise the torque resistance, in variable proportions ranging between +45° and -45°, depending on maximum torque direction;
2. 0° HM carbon/epoxy plies should be used in order to maximise the axial stiffness and minimise the axial damping;
3. 90° HM carbon/epoxy plies should be used far from the middle surface in order to maximise the torsional buckling torque;
4. the laminate does not generally have to be symmetrical.

References

[1] H. Zinberg, M. F. Symonds, The Development of an Advanced Composite Tail Rotor Driveshaft, in: Proceedings of the 26th Annual Forum of the American helicopter Society, Washington, United States, 1970.

[2] O. A. Bauchau, Optimal design of high speed rotating gaphite/epoxy shafts, Journal of Composite Materials 17 (3) (1983) 170–181.

[3] J. W. Lim, M. S. Darlow, Optimal sizing of composite power transmission shafting, Journal of the American Helicopters society 31 (1986) 75–83.

[4] R. F. Kraus, M. S. Darlow, W. P. Conley, P. L. Jones, Experimental verification of optimized helicopter driveshaft designs, in: Proceedings of the 2nd International Conference on Rotorcraft Basic Research, College Park, United States, 1988.

[5] M. S. Darlow, J. Creonte, Optimal design of composite helicopter power transmission shafts with axially varying fiber lay-up, Journal of the American Helicopters society 40 (2) (1995) 50–56.

[6] H. B. H. Gubran, K. Gupta, Composite Shaft Optimization Using Simulated Annealing, Part I: Natural Frequency, International Journal of Rotating Machinery 8 (4) (2002) 275–283.

[7] D. Goldberg, Genetic Algorithms, Addison Wesley, 1989.

[8] R. Le Riche, R. T. Haftka, Optimization of laminate stacking sequence for buckling load maximization by genetic algorithm, AIAA Journal 31 (5) (1993) 951–956.

[9] C. Roos, C. E. Bakis, Multi-Physics Design and Optimization of Flexible Matrix Composite Driveshafts, Composite Structures In Press, Accepted Manuscript.

[10] T. S. Brown, D. B. Rezin, Hybrid composite driveshaft design considerations, in: Proceedings of the Winter Annual Meeting for Modern developments in composite materials and structures, New York, United States, 1979.

[11] F.-J. Xu, J.-R. Ye, Y.-D. Xue, Design and Mechanical Analysis of a Hybrid Composite Driveshaft, Composite Structures 9 (1991) 207–216.

[12] D. G. Lee, H. S. Kim, J. W. Kim, J. K. Kim, Design and manufacture of an automotive hybrid aluminum/composite drive shaft, Composite Structures 63 (2004) 87–99.

[13] H. B. H. Gubran, Dynamics of hybrid shafts, Mechanics Research Communications 32 (4) (2005) 368–374.

[14] C. Hochard, Optimum design of laminated composite structures, Composite Structures 63 (2) (2004) 159–165.

[15] C. Hochard, J. Payan, O. Montagnier, Design and computation of laminated composite structures, Composites Science and Technology 65 (2005) 467–474.

[16] O. Montagnier, C. Hochard, Compression characterization of high modulus carbon fibers, Journal of Composite Materials 39 (2005) 35–49.

[17] J. K. Dutt, B. C. Nakra, Stability of rotor systems with viscoelastic supports, Journal of Sound and Vibration 153 (1) (1992) 89–96.

[18] O. Montagnier, C. Hochard, Dynamic instability of supercritical driveshafts mounted on dissipative supports – effect of viscous and hysteretic internal damping, Journal of Sound and Vibration 305 (2007) 378–400.

[19] J. K. Dutt, B. C. Nakra, Stability characteristics of rotating systems with journal bearings on viscoelastic support, Mechanism and Machine Theory 31 (6) (1996) 771–779.

[20] C. W. Bert, C. K. Kim, Whirling of composite material driveshafts including bending-twisting coupling and transverse shear deformation, Journal of Vibration and Acoustics 117 (1) (1995) 7–21.
[21] S. P. Singh, K. Gupta, Composite shaft rotordynamic analysis using a layerwise theory, Journal of Sound and Vibration 191 (5) (1996) 739–756.
[22] H. B. H. Gubran, K. Gupta, The effect of stacking sequence and coupling mechanisms on the natural frequencies of composite shaft, Journal of Sound and Vibration 282 (1-2) (2005) 231–248.
[23] R. Sino, T. N. Baranger, E. Chatelet, G. Jacquet, Dynamic analysis of a rotating composite shaft, Composites Science and Technology 68 (2) (2008) 337–345.
[24] R. D. Adams, Engineering Material Handbook, vol. 1, chap. Damping properties analysis of composites, ASME, 206–217, 1987.
[25] O. Montagnier, Tubes composites à grande vitesse de rotation : analyses expérimentales et modélisation, Ph.D. thesis, University of Marseille, France, 2005.
[26] R. D. Adams, D. G. C. Bacon, Effect of fiber orientation and laminate geometry on the dynamic properties of the C.F.R.P., Journal of Composite Materials 7 (1973) 422–428.
[27] R. G. Ni, R. D. Adams, A rational method for obtaining the dynamic mechanical properties of laminae for prediction of the damping of laminated plates and beams, Composites 15 (3) (1984) 193–199.
[28] S. Tsai, H. Hahn, Introduction to composite materials, CRC, 1980.
[29] S. W. Tsai, E. M. Wu, A general theory of strength of anisotropic materials, Journal of Composite Materials 5 (1971) 58–69.
[30] C. Hochard, S. Miot, N. Lahellec, F. Mazerolle, M. Herman, J. Charles, Behaviour up to rupture of woven ply laminate structures under static loading conditions, Composites Part A 40 (8) (2009) 1017–1023.
[31] T. Hayashi, Optimization of the Torsional-Rigidity and Strength for Fiber Reinforced Composite Cylinders, in: Proceedings of the Conference on Composite Materials, vol. 1, 703–724, 1975.
[32] W. Flügge, Stresses in shells, Springer-Verlag, Berlin, 2nd edn., 1973.
[33] C. Bert, C.-D. Kim, Analysis of buckling of hollow laminated composite drive shaft, Composites Science and Technology 53 (1995) 343–351.
[34] K. Hibbitt, I. Sorensen, ABAQUS/Standard: User's Manual, Hibbitt, Karlsson & Sorensen, 2001.
[35] O. A. Bauchau, T. M. Krafchack, J. F. Hayes, Torsional Buckling Analysis and Damage Tolerance of Graphite/Epoxy Shafts, Journal of Composite Materials 22 (1988) 258–270.
[36] H. B. H. Gubran, K. Gupta, Composite Shaft Optimization Using Simulated Annealing, Part II: Strength and Stresses, International Journal of Rotating Machinery 8 (4) (2002) 285–293.
[37] The MathWorks, MATLAB, The MathWorks Inc., http://www.mathworks.com, 1990.
[38] O. Montagnier, C. Hochard, Design of hybrid high modulus/high resistance carbon fibers driveshafts — Subcritical and supercritical solutions, in: Proceedings of the 12th European Conference on Composite Materials, Biarritz, France, 2006.